# An Automatic Multi-level Gyro Calibration Architecture for Consumer Portable Devices

You Li[1,2,3], Jacques Georgy[2], Xiaoji Niu[3], Chris Goodall[2] and Naser El-Sheimy[1]
1 Department of Geomatics, University of Calgary
2 InvenSense Inc.
3 GNSS Research Center, Wuhan University

***Abstract*— A novel calibration architecture that calculates the gyro biases without any external equipment and without any user intervention is proposed. This architecture uses a Kalman filter algorithm and utilizes multi-level constraints, such as pseudo-observation updates and the accelerometer and magnetometer measurements. Walking tests with smartphones show that the proposed architecture is effective and accurate when being used under various scenarios with different phone contexts.**

***Keywords*—MEMS inertial sensors; IMU; Kalman filtering; indoor navigation; pedestrian navigation**

## I. INTRODUCTION

Advances in Micro-Electro-Mechanical Systems (MEMS) technology combined with the miniaturization of electronics have made it possible to produce chip-based sensors, such as inertial sensors (i.e., accelerometers and gyroscopes (gyros)) and magnetometers. MEMS chips are small and lightweight, consumes very little power, and are extremely low-cost [1]. By virtue of these advantages, MEMS sensors have become appropriate candidates for motion tracking and navigation (i.e., attitude, velocity, position, etc.) applications in many electronic devices such as smartphones, gaming systems, toys, and the next generation wearable devices. For consumer portable devices, dead reckoning (DR) is usually the navigation algorithm used to navigate with inertial sensors, thus the sensors are not dependent on the transmission or reception of signals from an external source. Such self-contained MEMS-based inertial sensors are ideal for providing continuous information for indoor/outdoor navigation [2].

However, the errors of low-cost MEMS inertial sensors change with time and are highly dependent on the conditions of the operational environment such as temperature [3]. Although lab calibration at room temperature is a useful way to remove many deterministic sensor errors [4], these sensors' readings contain also stochastic errors and the actual values of the sensor errors can differ due to the difference between the operational and calibration environments. In real world tests, the changes of the MEMS gyro biases can reach thousands of deg/h over the whole temperature range (-10~+70 $^{o}$C) [3]. Due to the integration process in the inertial navigation mechanization, such drifts will accumulate, resulting in increasing navigation errors. For indoor environments, position or velocity updates from GNSS are not always available. If this is the case, the navigation accuracy will degrade faster over time.

A quick and convenient in-field calibration is needed to mitigate the drift of the inertial sensor errors, especially the gyro biases. The calibration process should happen automatically in the background without the user intervention. This is because mainstream consumer and non-professional users should be able to benefit from the calibration and from a better navigation solution using the calibrated sensors without any specific requirement from them. Achieving such a calibration is not easy, especially when working with consumer-grade inertial sensors. Most calibration methods require external equipment or tools to provide a reference for calibration. It is not realistic to expect the users of the electronic products to use a separate tool to calibrate the sensors. Furthermore, current traditional methods to calibrate the inertial sensors without an external tool involve: (i) using static periods for gyroscopes calibration when the sensors are fully static; and (ii) using the gravity vector for accelerometer calibration while ensuring that the IMU covers various attitudes to make sure that the system is observable [5-8]. The need for static periods limits the scenarios where calibration can happen. The need for various attitudes increases the operation complexity. Furthermore, when the calibration is done automatically in the background, the need for various attitudes will delay having a full calibration without user involvement to do specific motions.

In this paper, an efficient calibration architecture is proposed to calculate the gyro biases without any external equipment and without any user intervention. This architecture uses a Kalman filter algorithm and utilizes multi-level constraints to improve the efficiency and accuracy of the calibration. These constraints are used adaptively based on automatic motion detection algorithms.

This paper is organized as follows. Section II reviews the previous relevant works. Section III explains the methodology of this new architecture, including the details of various constraints. Section IV shows some results with analysis and Section V draws the conclusion.

## II. PREVIOUS WORKS

The commonly used calibration methods include the standard calibration methods [4, 9] and the multi-position calibration methods [5-7, 10, 11]. Due to the dependence on specialized equipment, the standard methods are always designed for in-lab tests, factory calibration and relatively high-grade IMUs. To calibrate an IMU just with simple devices or even without any specific tool, a multi-position method is developed. The basic idea of a multi-position method can be stated as follows: the norms of the measured outputs of the accelerometer and gyro cluster are equal to the magnitudes of the given specific force (i.e.

978-1-4673-8054-6/14/$31.00 ©2014 IEEE

gravity) and rotational velocity inputs (i.e. the earth rotation), respectively [12]. However, the main drawback in using multi-position calibration method is that the gyro reference (earth rotation rate) is a weak signal (15 deg/h) which can result in observability problems when estimating the scale factors and non-orthogonalities. Therefore, a single axis turntable is required to provide a strong rotation rate signal [6, 7, 10, 11], which limits the multi-position method to laboratories. To estimate gyro errors without any external equipments, an in-field calibration method is developed [8]. The accelerometer triad was first calibrated by the multi-position method through multiple quasi-static states generated by hand holding. Then the outputs from the calibrated accelerometers can be used to calibrate gyros. To avoid the requirement of being static/quasi-static, we have presented an in-situ hand calibration method [13]. By introducing a kind of pseudo-observations, this method is efficient to calibrate both the biases and scale factors of both gyros and accelerometers without any external tool; however, it is based on the premise that the IMU is rotated approximately around its measurement center by hand, which needs user intervention.

This paper tries to remove the inconvenient user intervention process. Multiple constraints are utilized to provide an efficient and accurate calibration solution.

## III. METHODOLOGY

Multiple levels of constraints are used in the proposed calibration architecture. The first level is called pseudo-observation updates. This constraint is activated when the change in position between two time epochs is within a limited range. Such cases are detected by the automatic motion detection routine. In this case, the constraints □r = constant and □v = 0 are regarded as an observation of *pseudo-position* and *pseudo-velocity*. The actual position and velocity changes during the calibration process are embodied in the covariance matrix of measurement noise (R) in the Kalman Filter. The R matrix is tuned adaptively according to the IMU outputs. The use of the pseudo-observation updates makes it possible to calculate the gyro errors without any external equipment or tools. Also, the pseudo-observation updates can be used while the user moves naturally. Thus, it is feasible to run the calibration algorithm in the background without any user interaction.

The second level of constraints is from the accelerometers and magnetometers. The update information for the Kalman Filter can be obtained from either the accelerometer-measured specific forces or the accelerometer-derived roll and pitch. The former is regarded as the tightly-coupled method, while the latter is regarded as the loosely-coupled method. The R matrix for the accelerometer measurements are tuned adaptively based on the magnitude of the actual linear acceleration. Using magnetometer measurements presents a similar process.

The algorithm is comprised of the IMU sensor error models, the Kalman filter models and the INS mechanization. The INS mechanization applied in this paper follows [14] and will not be described in detail in this paper. For details about Kalman filter the reader can refer to [15].

The proposed calibration architecture is different from the traditional method which adds sensor errors into the navigation Kalman filter. The main objective of the navigation algorithm is to estimate the navigation states (i.e., position, velocity, and attitude) instead of sensor errors. Therefore, when using extra apriori information or setting the parameters, it is preferable to assure that any inaccurate estimate of sensor errors will not destroy the navigation algorithm rather than to estimate residual sensor errors with a higher accuracy. However, in the calibration architecture, we use specific updates, such as the pseudo-observations, and set the parameters of the Kalman filter with the aim of maximizing the calibration accuracy. Also, the calibration results can be evaluated before feedback to avoid the degradation of the whole navigation system under extreme navigation conditions.

The following sub-sections will introduce the algorithm, including system error models, the system model and the measurement model (for updates from multiple sensors and priori information).

### A. Sensor Error Models

A major problem of applying MEMS sensors is the changes of the biases and the scale factors due to temperature variations [3]. Given the current MEMS manufacturing technology, non-orthogonality errors are relatively smaller compared to other errors. Therefore only biases and scale factor errors are taken into account in the calibration algorithm.

Involving the biases and linear scale factor errors, the output error equations of accelerometers and gyros can be described respectively as below:

$$\delta \mathbf{f}^b = \mathbf{b}_a + diag(\tilde{\mathbf{f}}^b)\delta \mathbf{s}_a + \mathbf{w}_a \quad (1)$$

$$\delta \boldsymbol{\omega}_{ib}^b = \mathbf{b}_g + diag(\tilde{\boldsymbol{\omega}}_{ib}^b)\delta \mathbf{s}_g + \mathbf{w}_g \quad (2)$$

where $\delta \mathbf{f}^b$ and $\delta \boldsymbol{\omega}_{ib}^b$ are the error vectors of specific force and angular rate respectively. $\mathbf{b}_a$ and $\mathbf{b}_g$ are the bias vectors of the accelerometers and the gyros. $\delta \mathbf{s}_a$ and $\delta \mathbf{s}_g$ are the linear scale factor error vectors, $\mathbf{w}_a$ and $\mathbf{w}_g$ represent the sensor noises. $\tilde{\mathbf{f}}^b$ and $\tilde{\boldsymbol{\omega}}_{ib}^b$ are the measured specific force and angular rate, respectively. The symbol $diag(\cdot)$ indicates the diagonal matrix form of a vector.

The sensor biases and scale factor errors are modeled as first-order Gauss-Markov processes [16]. Take the gyro biases as an example:

$$\dot{\mathbf{b}}_g = -\frac{1}{\tau_{bg}}\mathbf{b}_g + \mathbf{w}_{bg} \quad (3)$$

where $\tau_{bg}$ denotes for the correlation time of the gyro biases, $\mathbf{w}_{bg}$ is the driving noises.

### B. Kalman Filter System Model

A simplified form of the INS error model [14] is applied as the continuous-time state equations in the Kalman filter [13].

$$\begin{bmatrix} \delta\dot{\mathbf{r}}^n \\ \delta\dot{\mathbf{v}}^n \\ \dot{\boldsymbol{\psi}} \end{bmatrix} = \begin{bmatrix} -\boldsymbol{\omega}_{en}^n \times \delta\mathbf{r}^n + \delta\mathbf{v}^n \\ -(2\boldsymbol{\omega}_{ie}^n + \boldsymbol{\omega}_{en}^n)\times\delta\mathbf{v}^n + \mathbf{f}^n \times \boldsymbol{\psi} + \mathbf{C}_b^n \delta\mathbf{f}^b \\ -(\boldsymbol{\omega}_{ie}^n + \boldsymbol{\omega}_{ec}^n)\times\boldsymbol{\psi} - \mathbf{C}_b^n \delta\boldsymbol{\omega}_{ib}^b \end{bmatrix} \quad (4)$$

where $\delta\mathbf{r}^n$, $\delta\mathbf{v}^n$ and $\boldsymbol{\psi}$ are the position error, the velocity error, and the attitude error. $\mathbf{C}_b^n$ is the Direction Cosine Matrix from b-frame (i.e., the body frame) to n-frame (i.e., the navigation frame). $\mathbf{f}^n$ is the specific force vector projected to c-frame, and $\boldsymbol{\omega}_{ie}^n$ and $\boldsymbol{\omega}_{en}^n$ represent the angular velocity of the earth and the angular rate vector of c-frame with respect to e-frame (i.e. the Earth frame), both projected to c-frame. The symbol " $\times$ "denotes cross product of two vectors. $\delta\mathbf{f}^b$ and $\delta\boldsymbol{\omega}_{ib}^b$ are the accelerometer error and gyro error explained in equation (1) and (2).

### C. Kalman Filter Measurement Model

Different kinds of constraints are used to build the measurement model to enhance the calibration. The measurement uncertainties are embodied in the measurement noise matrix ( $\mathbf{R}$ ) of the Kalman filter.

#### 1) Pseudo-observations

The pseudo-position or pseudo-velocity observation can be written as follows [13]:

$$\hat{\mathbf{r}}^n - \tilde{\mathbf{r}}^n = \delta\mathbf{r}^n + \mathbf{n}_r \quad (5)$$

with $\tilde{\mathbf{r}}^n = \mathbf{constant}$

or

$$\hat{\mathbf{v}}^n = \delta\mathbf{v}^n + \mathbf{n}_v \quad (6)$$

where $\hat{\mathbf{r}}^n$ and $\hat{\mathbf{v}}^n$ are position and velocity vectors predicted by the INS mechanization; $\tilde{\mathbf{r}}^n$ is the observation vectors of the proposed pseudo-position and pseudo-velocity, respectively; $\delta\mathbf{r}^n$ and $\delta\mathbf{v}^n$ are the position errors and velocity errors. $\mathbf{n}_r$ and $\mathbf{n}_v$ are the measurement noises (i.e. the inaccuracy) of the pseudo-position and pseudo-velocity.

A feasible way of setting the $\mathbf{R}$ matrix for the pseudo-observations is provided here. First a set of initial position and velocity noises are given roughly; and then the position or velocity changes during a period can be calculated; based on this result, the elements in $\mathbf{R}$ could be further adjusted. This process runs autonomously.

#### 2) Accelerometer and Magnetometer measurement updates

Accelerometers and magnetometers can also be used to determine attitude; however, both of them suffer from big short term noises [17]. Therefore, accelerometers and magnetometers are integrated with gyros to provide robust attitude solutions in many application of attitude and heading reference systems (AHRS) [18]. The details of using the accelerometer and magnetometer measurements can refer to [17].

#### 3) Initial Alignment

The initial DCM $\hat{\mathbf{C}}_b^n(t_0)$ can be determined by using the accelerometer and magnetometer measurements as [19]

$$\hat{\mathbf{C}}_b^n = \left(\begin{bmatrix} \mathbf{f}^n & \mathbf{m}^n & \mathbf{r}^n \end{bmatrix}^T\right)^{-1} \begin{bmatrix} \tilde{\mathbf{f}}^b & \tilde{\mathbf{m}}^b & \tilde{\mathbf{r}}^b \end{bmatrix}^T \quad (7)$$

## IV. Tests and Results

Several walking trajectories were collected. The trajectories comprised different phone locations and attitudes including handheld, at ear, dangling, in pocket, and in backpack. At the end of each test, there was a quasi-static period (holding by hand) to calculate a reference of gyro biases. The tests were performed with three Samsung Galaxy SIII smartphones. To make the gyro errors more significant (i.e., to test the calibration algorithm), gyro biases of 3 deg/s, -3 deg/s and 3 deg/s have been added into the raw output of the gyros before the data processing. One test trajectory is shown in Figure 1.

Figure 1. Test trajectory

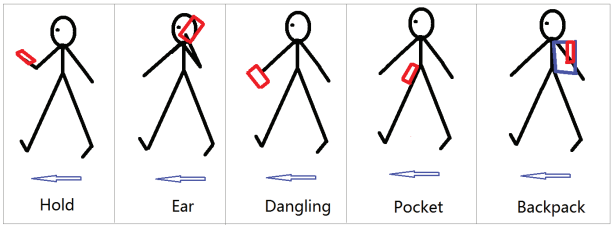


Figure 2. Tested scenarios

The figures of the calibraiton results with phone #1 are shown in TABLE I. , while those with phone #2 and #3 are shown in TABLE II. The solid line at the end of each curve indicates the reference value calculated from the quasi-static data.

TABLE I. Figures of Calibration Results with Phone #1

| Scenarios | Typical IMU outputs | Results (phone #1) |
|---|---|---|
| Hold | 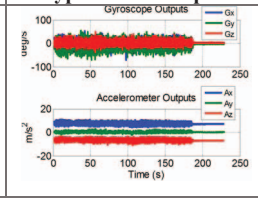 | 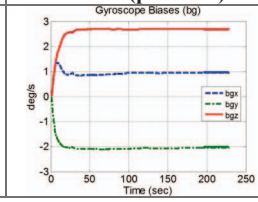 |

| | | |
|---|---|---|
| Ear | 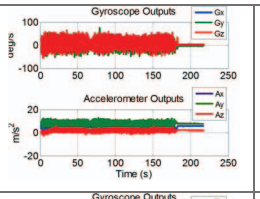 | 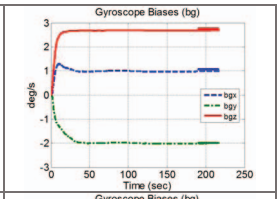 |
| Dangling | 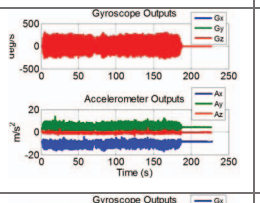 | 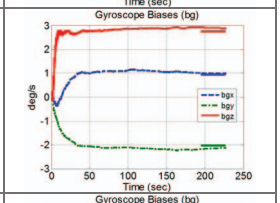 |
| Pocket | 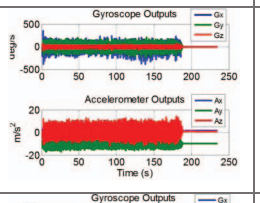 | 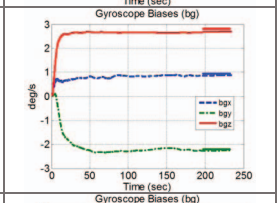 |
| Backpack | 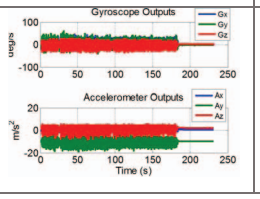 | 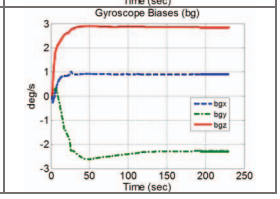 |

TABLE II. FIGURES OF CALIBRATION RESULTS WITH PHONE #2 AND #3

| Scenarios | Results (phone #2) | Results (phone #3) |
|---|---|---|
| Hold | 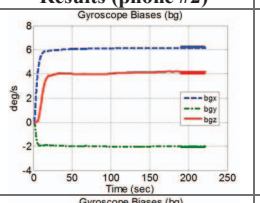 | 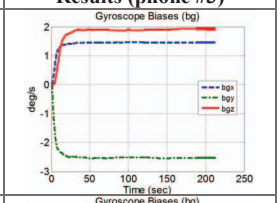 |
| Ear | 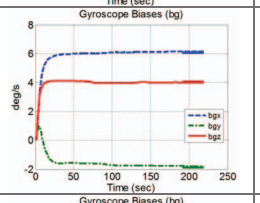 | 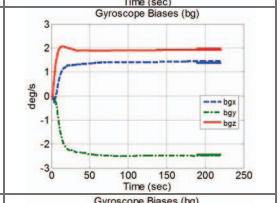 |
| Dangling | 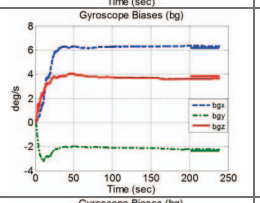 | 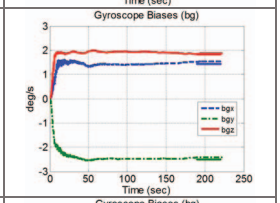 |
| Pocket | 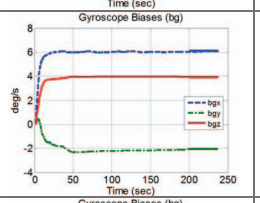 | 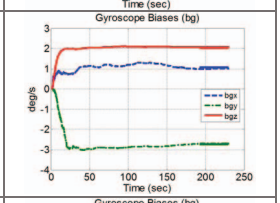 |
| Backpack | 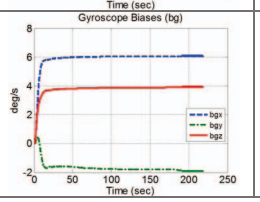 | 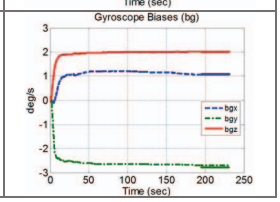 |

Most of the calibrated sensor errors have converged in the first 30 s, and all of them converged within 60 s. TABLE III. shows the statistical results of the sensor errors under all scenarios with different phones. The RMS values were calculated using the differences between the calibration results at every epoch after convergence and the reference values.

TABLE III. STATISTICAL RESULTS OF THE CALIBRATION ERRORS UNDER ALL SCENARIOS

| Phone | Values (deg/s) | X | Y | Z |
|---|---|---|---|---|
| #1 | Reference | 0.971 | -2.099 | 2.776 |
| | RMS | **0.075** | **0.085** | **0.077** |
| #2 | Reference | 6.173 | -2.017 | 3.981 |
| | RMS | **0.085** | **0.093** | **0.084** |
| #3 | Reference | 1.291 | -2.587 | 1.973 |
| | RMS | **0.066** | **0.063** | **0.059** |

The proposed calibration architecture can reduce the gyro biases from several deg/s to under 0.1 deg/s. Although the sensors within different phones have different errors (e.g., the phone #2 have larger sensor errors after adding ± 3 deg/s), the results are all at the same level and acceptable.

Also, we calculated the statistical results under different use cases. The results are shown in TABLE IV.

TABLE IV. STATISTICAL RESULTS OF THE CALIBRATION ERRORS UNDER ALL SCENARIOS

| Motions | RMS (deg/s) | | |
|---|---|---|---|
| | X | Y | Z |
| Hold | **0.067** | **0.039** | **0.056** |
| Ear | **0.060** | **0.073** | **0.076** |
| Dangling | **0.096** | **0.127** | **0.119** |
| Pocket | **0.104** | **0.097** | **0.080** |
| Backpack | **0.051** | **0.089** | **0.045** |

The RMS values for dangling and pocket are larger than those for the other motions. This meets our expectation, since both dangling and pocket provide stronger smartphone dynamics, as shown in the IMU outputs in TABLE I. Even under such challenging conditions, the proposed method provides results which is acceptable for MEMS sensors.

## V. CONCLUSION

With the proposed calibration architecture, the gyro biases of smartphones were reduced from several deg/s to approximate 0.1 deg/s or lower when walking and with various phone use cases (i.e., handheld, ear, dangling, pocket, and backpack). This calibration architecture works in real-time and has a lot of potential for calibration of the MEMS gyros within consumer electronics.

## AKNOWLEDGEMENTS

This work was supported in part by National Natural Science Foundation of China (41174028) and the research funding from Dr. Naser El-Sheimy. The first author (YL) would also thank the China Scholarship Council for its support (No. 201306270139).

## REFERENCES


1. El-Sheimy, N., *Lecture note 623 - Inertial Techniques and INS/DGPS Integration, Department of Geomatics Engineering, University of Calgary*. 2014.
2. Shaeffer, D.K., *MEMS inertial sensors: A tutorial overview.* Communications Magazine, IEEE, 2013. **51**(4): p. 100-109.
3. Niu, X., Y. Li, H. Zhang, Q. Wang, and Y. Ban, *Fast Thermal Calibration of Low-Grade Inertial Sensors and Inertial Measurement Units.* Sensors, 2013. **13**(9): p. 12192-12217.
4. Titterton, D.H. and J.L. Weston, *Strapdown inertial navigation technology -2nd ed.* 2004: the Institution of Electrical Engineers, London, United Kingdom.
5. Lötters, J., J. Schipper, P. Veltink, W. Olthuis, and P. Bergveld, *Procedure for in-use calibration of triaxial accelerometers in medical applications.* Sensors and Actuators A: Physical, 1998. **68**(1): p. 221-228.
6. Skog, I. and P. Händel. *Calibration of a MEMS inertial measurement unit*. in *XVII IMEKO World Congress*. 2006.
7. Syed, Z., P. Aggarwal, C. Goodall, X. Niu, and N. El-Sheimy, *A new multi-position calibration method for MEMS inertial navigation systems.* Measurement Science and Technology, 2007. **18**(7): p. 1897.
8. Fong, W., S. Ong, and A. Nee, *Methods for in-field user calibration of an inertial measurement unit without external equipment.* Measurement Science and Technology, 2008. **19**(8): p. 085202.
9. Xiao, L., S. Wei, and W. Sun, *Research on the high accuracy rapid test method of IMU.* J. Astronaut., 2008. **29**: p. 172-177.
10. Zhang, H., Y. Wu, W. Wu, M. Wu, and X. Hu, *Improved multi-position calibration for inertial measurement units.* Measurement Science and Technology, 2010. **21**(1): p. 015107.
11. Nieminen, T., J. Kangas, S. Suuriniemi, and L. Kettunen, *An enhanced multi-position calibration method for consumer-grade inertial measurement units applied and tested.* Measurement Science and Technology, 2010. **21**(10): p. 105204.
12. Shin, E. and N. El-Sheimy, *A new calibration method for strapdown inertial navigation systems.* Z. Vermess, 2002. **127**: p. 1-10.
13. Li, Y., X. Niu, Q. Zhang, H. Zhang, and C. Shi, *An in situ hand calibration method using a pseudo-observation scheme for low-end inertial measurement units*. Measurement Science and Technology, 2012. **23**(10): p. 105104.
14. Shin, E.-H., *Estimation techniques for low-cost inertial navigation*, in *Department of Geomatics Engineering*. 2005, University of Calgary: Calgary, Canada.
15. Brown, R.G. and P.Y.C. Hwang, *Introduction to random signals and applied Kalman filtering*. Vol. 1. 1992: John Wiley & Sons New York.
16. Maybeck, P.S., *Stochastic models, estimation, and control*. Vol. 3. 1982: Access Online via Elsevier.
17. Han, S. and J. Wang, *A novel method to integrate IMU and magnetometers in attitude and heading reference systems.* Journal of Navigation, 2011. **64**(4): p. 727-738.
18. Li, W. and J. Wang, *Effective adaptive Kalman filter for MEMS-IMU/magnetometers integrated attitude and heading reference systems.* Journal of Navigation, 2013. **66**(01): p. 99-113.
19. Saxena, A., G. Gupta, V. Gerasimov, and S. Ourselin. *In use parameter estimation of inertial sensors by detecting multilevel quasi-static states*. in *Knowledge-Based Intelligent Information and Engineering Systems*. 2005. Springer.